Volume 11, Number 2, 2018. pp. 115-124

Jordan Journal of Physics

ARTICLE

Analysis of the Force Exerted on an Accelerated Beam of Electrons by Its Own Wakefield in the Laser-Driven Rf-gun

N. M. Ershaidat[a] and **W. Salah**[b]

[a] *Physics Department, The University of Jordan, Amman 11942, Jordan.*
[b] *Physics Department, The Hashemite University, Zarqa 13115, Jordan.*

Received on: 9/9/2017; *Accepted on: 12/12/2017*

Abstract: Analytical expressions for the wakefield force acting on an electrons beam, in the RF-photoinjector, during the beam extraction from the cathode, are derived. These expressions are obtained by taking space charge effects and beam motion into account. The former is described in terms of the field's components due to Lienard-Wiechert potential and the method of images, close to the cathode surface. The beam motion is emphasized circumstantiating the fast transition, owing to quick acceleration by the high gradient RF-accelerating field, from thermal velocity, near the immediate vicinity of the cathode, to a non-relativistic velocity at the end of the photoemission. Numerical investigation of the beam wakefield force elicited two significant effects on the beam: the first one, attributable to the longitudinal component of the force, influences the trailing electrons in the beam and changes the energy of the individual electrons, depending on their position. The second one, attributable to the transverse component of the force, deflects the beam trajectory. After all, the electrons within the beam feel, over the beam length, an average deflecting force that is proportional to the radial displacement.

Keywords: Free electron laser, Beam dynamics, Wakefields, RF-photoinjector.
PACS: 41.75.Jv Laser-driven acceleration, 41.75 Lx Other advanced accelerator concepts, 41.75.Ht Relativistic electron and positron beams.

Introduction

The performance of lasing operation of free electron laser (FEL) [1-2] and laser- Compton X-ray [3-5] is based on the so-called self-amplified spontaneous emission (SASE) principle. The achievement of X-ray-SASE-FELs notably requires high beam brightness that is currently beyond the state of the art in addition to very low beam emittance [6-7]. Nowadays, laser-driven radio-frequency electron guns are substantially used to generate intense beams with low emittance and high brightness near the thermal source limit [8-9]. Usually, the emittance is defined as a statistical value in phase space [10–13], while the brightness is defined as the ratio of the beam current to the emittance [14-15]. During the emission as well as the acceleration of the electrons beam from the cathode to the accelerator exit, the beam qualities are degraded by the so-called wakefield.

In non-relativistic regime, the wakefield is the sum of the space charge field and the beam induced field. In ultra-relativistic regime, the wakefield has been addressed numerically, in the last two decades, by many authors using computer codes, such as MAFIA TS3 [16] and ASTRA [17]. The former code calculates the space charge forces of the beam itself; it includes the interaction of the charged particles with the surrounding structure. Despite the accurate results obtained by MAFIA, it is restricted in its application to short sections of the injector due to memory consumption, computation time and

Corresponding Author: Nidal M. Ershaidat **Email**: n.ershaidat@ju.edu.jo

numerical noise. The latter code is able to calculate large parts of the accelerator, but it does not take the interaction between the electrons in the beam and the surrounding structure into account. Inappropriately, an unwary common assumption in these codes was the invariance of beam velocity, these codes assuming that the photoelectrons are emerging from the cathode at the speed of light, in congruousness to a situation like that faced in photoinjectors, where the photoelectron beam is hurriedly accelerated by the strong RF-field applied at the cathode surface and attending relativistic velocity at the exit of the photoinjector. Therefore, the electrodynamics of the effects of acceleration-radiation field must be taken into account, in addition to the field produced by the electron beam itself [18].

Over the years, only few works involving the idea of a wakefield driven by an accelerated electron beam are found in the literature [19]. As an example, W. Salah and co-workers have intensely derived analytical expressions for the wakefield driven by an accelerated electron beam in the RF-photoinjector cavity [19-24]. In these works, the beam is traveling substantially with variable velocity less than the velocity of light and hence Kim monokinetic approximation [25] is far from being applied.

On the other hand, the space charge effects and the beam-induced fields are significant within 1cm of the cathode, where the beam is at low energy. At this stage, non-relativistic electrons are very sensitive to space-charge forces and the forces due to the field of the beam image in the cathode. Inside the pulse, electrons experience both longitudinal RF dynamics effects and wakefield effects, both effects leading to degrading the beam quality. The present work is devoted to the quantification of these effects.

In this paper, the authors' intent is to investigate numerically the short-range wakefield forces acting on the beam during the early beam transport; *i.e.,* emitted and strongly accelerated during its photoemission from the cathode. During the beam emission from the cathode, the self-field effects are not of space charge type, consequent to an electrostatic description in some beam proper frame. The self-field is an electromagnetic field, where relativistic effects of retardation and acceleration field play an important role. The wakefield force excited in this regime will be analyzed in some detail using Lienard-Weichert potential and the method of images [24]. This technique will be applied to parameters of the "ELSA" photoinjector facility [19] as shown in Fig. 1. As was justified in Ref. [23], we restrict our modelling to a ''pill-box'' type cavity. On the other hand, analytical and semi-empirical results [25-26] indicate that the influence of the exit hole can be neglected as long as $r_0/\Re << \frac{1}{3}$, where r_0 and $\Re$ are the hole and cavity radii, respectively (Fig. 1).

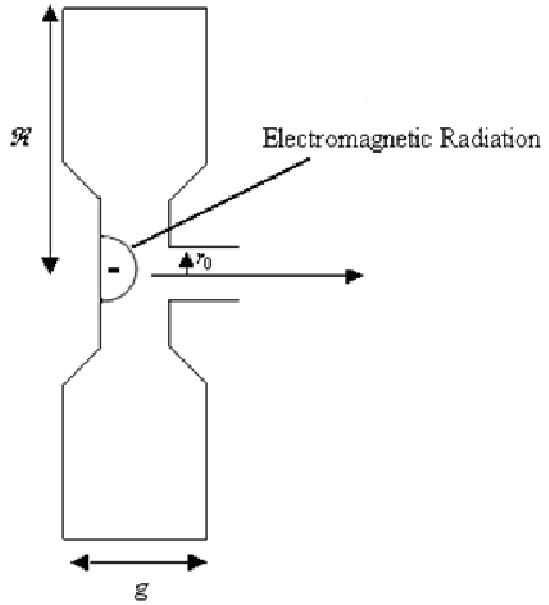

FIG. 1. "ELSA" photo-injector (144 MHz cavity).

Equations of Motion of the Beam of Electrons in RF-gun

It has been shown elsewhere [19] that the beam velocity $\vec{\beta}(z,t)$ and acceleration $\vec{\eta}(z,t)$ are parallel to the accelerated field $\vec{E}_0$ and independent of time. The beam velocity and longitudinal coordinates *z* are given by [19]:

$$\beta(z) = \frac{\sqrt{(1+Hz)^2 - 1}}{1+Hz} = \frac{dz}{c\,dt} \qquad (1)$$

The longitudinal coordinate of an electron at time *t*; *z*(*t*) is:

$$z(t) = \frac{1}{H}\left(\sqrt{1+(H\,c\,(t-t_z))^2} - 1\right) \qquad (2)$$

where t_z is the time at which element z of the beam leaves the photocathode and

$$H^{-1} = \frac{mc^2}{eE_0}. \tag{3}$$

Here, m is the mass of the electron at rest, e is the electron charge, E_0 is the amplitude of the accelerated field and c is the speed of light.

Theoretical Setup: Wakefield Maps

The wakefield components driven by an electron within the beam and the charge images on the cathode are reported elsewhere [24]. These components are obtained by a projection of Lienard-Wiechert fields on the axes illustrated in Fig. 2. As a result of cylindrical symmetry, the non-vanishing components of the electromagnetic fields are given by [24] as:

$$E_{z,\beta}(P,t|W) = \frac{e}{4\pi\varepsilon_0}\frac{\zeta' - z + \beta'\sqrt{s^2+(\zeta'-z)^2}}{\gamma'^2\,(\sqrt{s^2+(\zeta'-z)^2}+\beta'(\zeta'-z)^2)^3} \tag{4}$$

$$E_{z,\dot\beta}(P,t|W) = \frac{e}{4\pi\varepsilon_0 c}\frac{\dot\beta' s^2}{(\sqrt{s^2+(\zeta'-z)^2}+\beta'(\zeta'-z)^2)^3} \tag{5}$$

$$E_{r,\beta}(P,t|W) = \frac{e}{4\pi\varepsilon_0}\frac{s\cos\theta}{\gamma'^2\,(\sqrt{s^2+(\zeta'-z)^2}+\beta'(\zeta'-z)^2)^3} \tag{6}$$

$$E_{r,\dot\beta}(P,t|W) = -\frac{e}{4\pi\varepsilon_0 c}\frac{\dot\beta'(\zeta'-z)s\cos\theta}{(\sqrt{s^2+(\zeta'-z)^2}+\beta'(\zeta'-z)^2)^3} \tag{7}$$

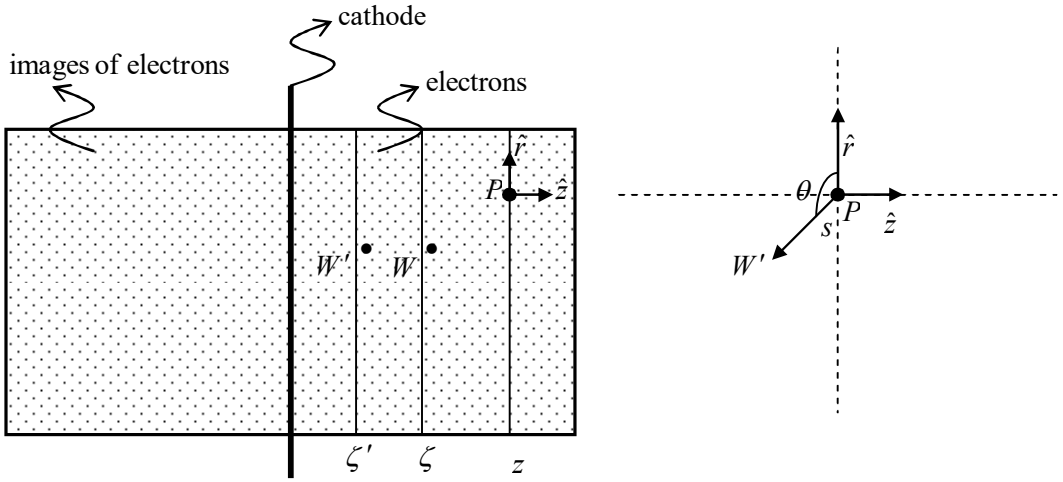

FIG. 2. Cylindrical coordinates s, θ and z. The unit vectors $\hat r$, $\hat\theta$ and $\hat z$ at point P in the direction of increasing s, θ and z, respectively.

Here, β and $\dot\beta = \frac{\partial\beta}{\partial t}$ exhibit the field components' dependence on velocity and acceleration, respectively, ε_0 is the permittivity of free space and the superscript (′) denotes values taken at time t'. The electromagnetic fields generated at time t and point P, by an electron moving on a specified trajectory, depends on the retarded position $\vec{W}(t')$ of the electron at time t'. On the other hand, the image of charges on the cathode was obtained by [24] by using a set of symmetric charges $+e$ at each instant t with respect to the cathode. The field component due to these images is then derived by replacing $-e$ with e, β' with $\bar\beta' = -\beta$, $\dot\beta'$ with $\bar{\dot\beta}' = -\dot\beta'$ and with $\bar\zeta = -\zeta$.

Formulation of Global Fields

The global field is the sum of the fields due to the space charge and due to the image of charges in the cathode. The non-vanishing components of the field are given by [24] as:

$$E_z(P,t)=\frac{e}{4\pi\varepsilon_0}\int_{D(P,\zeta,t)}\frac{J}{e\beta c}\left(\frac{\zeta'-z+\beta'\sqrt{s^2+(\zeta'-z)^2}}{\gamma'^2\left(\sqrt{s^2+(\zeta'-z)^2}+\beta'(\zeta'-z)\right)^3}+\right.$$

$$\left.\frac{\dot{\beta}'\,s^2}{c\left(\sqrt{s^2+(\zeta'-z)^2}+\beta'(\zeta'-z)\right)^3}\right)\times\frac{\beta}{\beta'}\left(1-\frac{\beta'(z-\zeta')}{\sqrt{s^2+(z-\zeta')^2}}\right)s\,ds\,d\theta\,d\zeta'+$$

$$\frac{-e}{4\pi\varepsilon_0}\int_{\bar{D}(P,\zeta,t)}\frac{J}{-e\bar{\beta}c}\left(\frac{\bar{\zeta}'-z+\bar{\beta}'\sqrt{s^2+(\bar{\zeta}'-z)^2}}{\gamma'^2\left(\sqrt{s^2+(\bar{\zeta}'-z)^2}+\bar{\beta}'(\bar{\zeta}'-z)\right)^3}+\right.$$

$$\left.\frac{\dot{\bar{\beta}}'\,s^2}{c\left(\sqrt{s^2+(\bar{\zeta}'-z)^2}+\bar{\beta}'(\bar{\zeta}'-z)\right)^3}\right)\times\frac{\bar{\beta}}{\bar{\beta}'}\left(1-\frac{\bar{\beta}'(z-\zeta')}{\sqrt{s^2+(z-\bar{\zeta}')^2}}\right)s\,ds\,d\theta\,d\bar{\zeta}' \tag{8}$$

The transverse E_r and the azimuthal B_θ components are effortlessly obtained by [24] as:

$$E_r(P,t)=\frac{1}{4\pi\varepsilon_0 c}\left(\int_{D(P,\zeta,t)}J\left(\frac{s^2}{\beta'\gamma'^2\left(\sqrt{s^2+(z-\bar{\zeta}')^2}\right)\left(\sqrt{s^2+(\zeta'-z)^2}+\beta'(\zeta'-z)\right)^2}\right.\right.$$

$$\left.+\frac{s\,\dot{\beta}'(\zeta'-z)}{\beta' c\sqrt{s^2+(z-\bar{\zeta}')^2}\left(\sqrt{s^2+(\zeta'-z)^2}+\beta'(\zeta'-z)\right)^2}\right)\cos\theta\;ds\,d\theta\,d\zeta'+$$

$$\int_{\bar{D}(P,\zeta,t)}J\left(\frac{s^2}{\bar{\beta}'\gamma'^2\left(\sqrt{s^2+(z-\bar{\zeta}')^2}\right)\left(\sqrt{s^2+(\bar{\zeta}'-z)^2}+\bar{\beta}'(\bar{\zeta}'-z)\right)^2}+\right.$$

$$\left.\left.\frac{s\,\dot{\bar{\beta}}(\bar{\zeta}'-z)}{\bar{\beta}' c\sqrt{s^2+(z-\bar{\zeta}')^2}\left(\sqrt{s^2+(\bar{\zeta}'-z)^2}+\bar{\beta}'(\bar{\zeta}'-z)\right)^2}\right)\cos\theta\,s\,ds\,d\theta\,d\bar{\zeta}'\right) \tag{9}$$

$$B_\theta(P,t)=\frac{1}{4\pi\varepsilon_0 c^2}\Big(\int_{D(P,\zeta,t)} J\Big(\frac{s^2}{\gamma'^2\sqrt{s^2+(z-\bar{\zeta}')^2}\,(\sqrt{s^2+(\zeta'-z)^2}+\beta'(\zeta'-z))^2}+\frac{s^2\,\dot{\beta}'}{\beta' c\,(\sqrt{s^2+(\zeta'-z)^2}+\beta'(\zeta'-z))^2}\Big)\cos\theta\; ds\, d\theta\, d\zeta' \;+$$

$$\int_{\bar{D}(P,\zeta,t)} J\Big(\frac{s^2}{\gamma'^2\sqrt{s^2+(z-\bar{\zeta}')^2}\,(\sqrt{s^2+(\bar{\zeta}'-z)^2}+\bar{\beta}'(\bar{\zeta}'-z))^2}+\frac{s^2\,\dot{\bar{\beta}}}{\bar{\beta}' c\,(\sqrt{s^2+(\bar{\zeta}'-z)^2}+\bar{\beta}'(\bar{\zeta}'-z))^2}\Big)\cos\theta\; s\, ds\, d\theta\, d\bar{\zeta}'\Big) \tag{10}$$

where $D(P,\zeta,t)$ represents a disc located within the beam.

$\vec{J}(r,z,t)$ is the current density which is related to the charge density by:

$$\rho(r,z,t)=\frac{I\varpi(z,t)}{\pi a^2\beta(z)c}\left[1-\Theta(r-a)\right]$$
$$\vec{J}(r,z,t)=\beta(z)c\,\rho(r,z,t)\,\vec{u}_z \tag{11}$$

Here, $\beta(z)=v(z)/c$ denotes the time-independent velocity, I is the total current whose axial profile $\varpi(z, t)$ is uniform and Θ (r-a) is the Heaviside step function.

$$t=\frac{1}{c}\sqrt{\zeta\,(\zeta+\frac{2}{H})} \tag{12}$$

$$t'=t-\frac{WP}{c}=t-\frac{1}{c}\sqrt{s^2+(z-\zeta)^2} \tag{13}$$

All the distances s must satisfy the following inequality:

$$s\le s_{\max}=\sqrt{(ct-\sqrt{\zeta\,(\zeta+\frac{2}{H})})^2-(\zeta-z)^2} \tag{14}$$

with

$$\zeta\le\frac{(ct+z)^2}{2(H^{-1}+z+ct)}=\zeta_{\max}\le z_H \tag{15}$$

where z_H is the longitudinal coordinates of the beam head.

Here, couples $(s,\bar{\zeta})$ represent a subset of points in the space of images. An electromagnetic signal is emitted at time t' and arrives to point P at time t. At this time t, all electrons own a longitudinal coordinate within z_H. To that end, we must have $\zeta_{\max}\le z_H$ and $s_{\max}$ does not exist unless $\zeta\le\zeta_{\max}$ as well as

$$\bar{\zeta}\;\le\;-\frac{(ct-z)^2}{2(ct+H^{-1}-z)}=\bar{\zeta}_{\max} \tag{16}$$

The Short-Range Wakefield Force Exerted on the Beam

The electromagnetic fields $\vec{E}$ and $\vec{B}$ induced by the beam are known as short-range wakefields. These fields act back on the beam and influence its motion. The Lorentz force acting on an amount of charge dq within the beam with cylindrical symmetry of radius a and total length $Z_H - Z_B$ is:

$$d\vec{F}=dq\,(E_z\,\hat{z}+E_r\,\hat{r})+dq\,\beta c\,\hat{z}\times B\,\hat{\theta} \tag{17}$$

where Z_H and Z_B are the longitudinal coordinates of the beam head and tail, respectively.

Given that:

$$dq = \rho(r,z,t)\, dV \quad (18)$$

Then, equation (17) becomes

$$d\vec{F} = \rho(r,z,t)[E_z\, \hat{z} + (E_r - \beta c\, B_\theta)\hat{r}\,]dV \quad (19)$$

Here, dV is the element of volume in cylindrical coordinates.

Numerical Results and Discussion.

Mathematica® is used in order to calculate the components of the force on the beam at different stages of the photo-emission of the beam from the cathode.

For numerical calculation of the wakefield forces, the following parameters, which are also harmonious with the ''ELSA'' facility, are adopted: I = 100 A, electron beam cross-sectional area πa^2 =1 cm^2 (a is the radius of the beam), beam time length τ = 100 ps and the accelerated field E_0 = 30 MV/m. These forces will be displayed as a function of the longitudinal reduced coordinates $Z = Hz$, $A = Ha$, $R = Hr$ and $T = Hc\tau$ based on the characteristic length H^{-1} (Eq. 3).

Wakefield and Wakefield Force at Different Emission Times

Figs. 3 and 4 display the longitudinal and transverse force acting on the beam, while Fig. 5 displays the total force acting on the beam at time $T = 2Hc\tau/5$. Figs. 6, 7 and 8 repeat Figs. 3, 4 and 5, but at time $T = Hc\tau$ (at the end of the photoemission). Figs. 3 and 6 indicate that the beam is found to be attracted towards the cathode by the positive field due to the images of charge on the cathode. This attractive force varies along the beam length; it is strongest on the drive electrons and decreasing as one moves from the beam head towards the trailing electrons. Figs. 4 and 7 show the salient features of the radial force on the entire beam. Briefly, the beam is defocusing towards the negative radial direction and the defocusing of the trailing electrons is less than that of driving ones. The transverse forces on the different slices of the beam along the beam lead to an augmentation in the transverse momentum of the beam. This augmentation is incoherent from the beam tail to the beam head. Consequently, the transverse phase space of the beam will be distorted and this distortion may alleviate the growth of the beam instability and brightness.

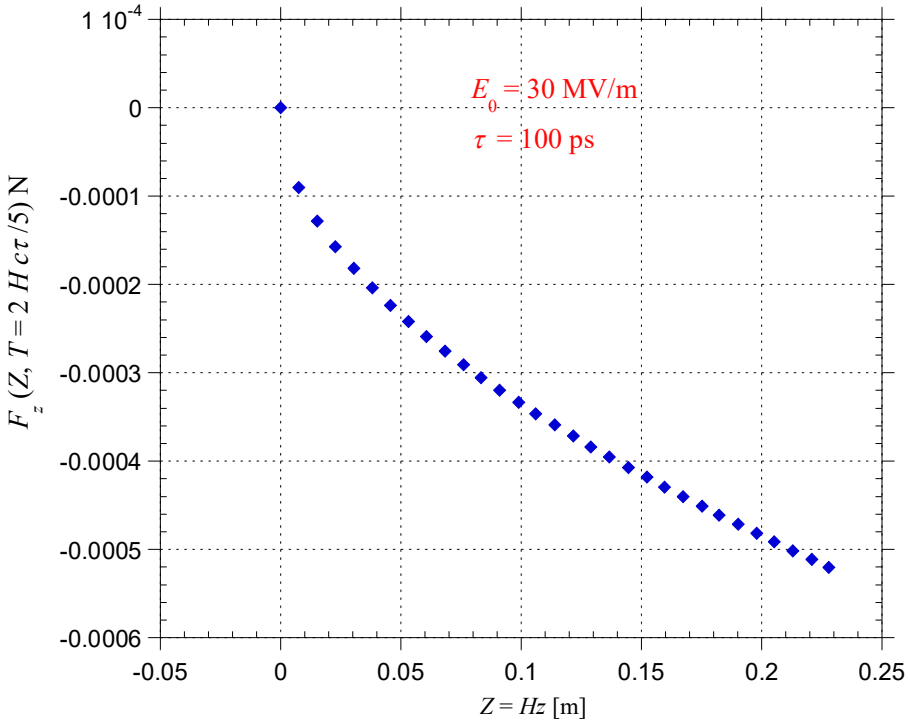

FIG. 3. Longitudinal component of the force acting on the beam as a function of the reduced coordinates Z along the axis of the RF-gun at time T = 2Hcτ / 5.

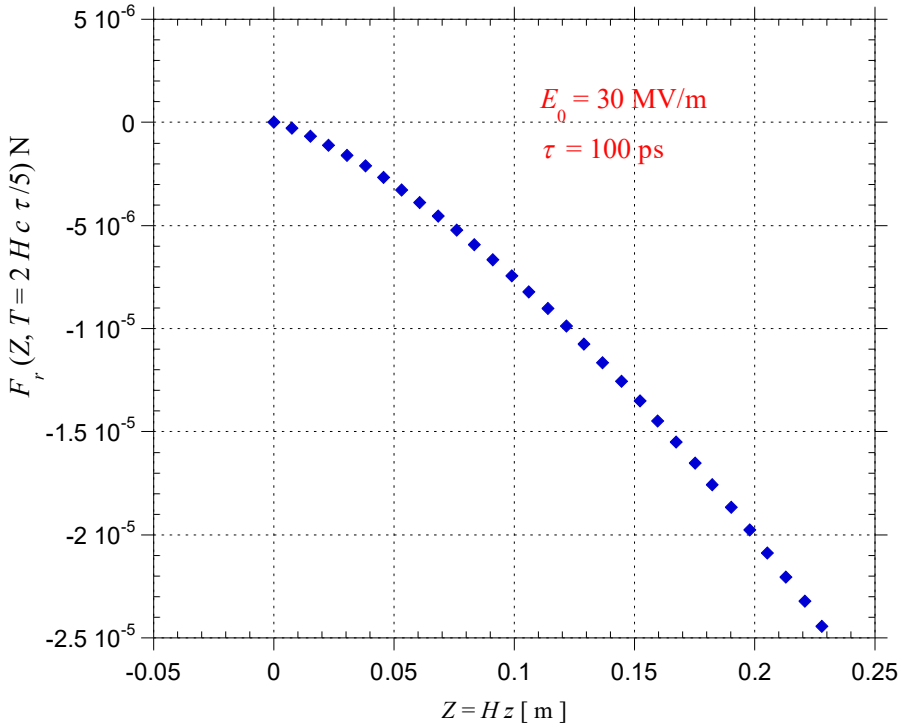

FIG. 4. Transverse component of the force acting on the beam as a function of the reduced coordinates Z along the axis of the RF-gun at time T = 2Hcτ / 5.

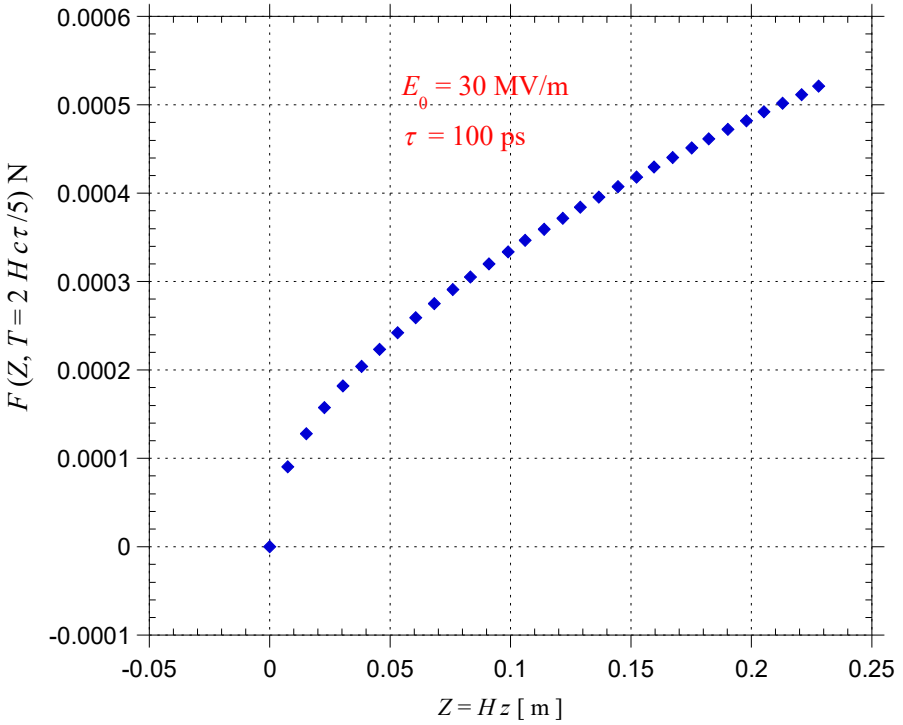

FIG. 5. Total force acting on the beam as a function of the reduced coordinates Z along the axis of the RF-gun at time T = 2Hcτ / 5.

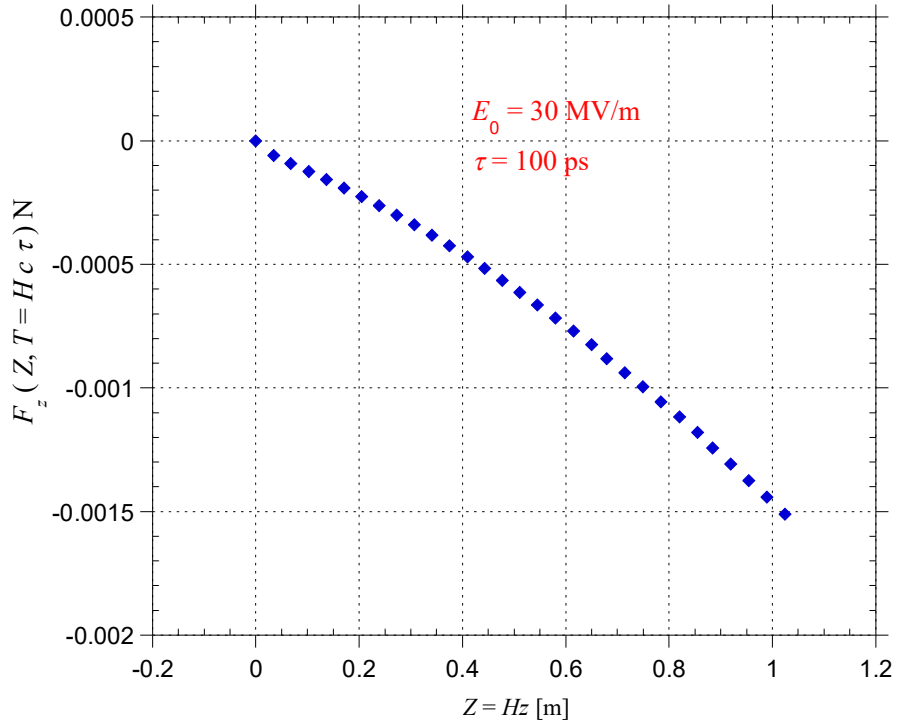

FIG. 6. Longitudinal component of the force acting on the beam as a function of the reduced coordinates Z along the axis of the RF-gun at the end of photoemission (at time T = Hcτ).

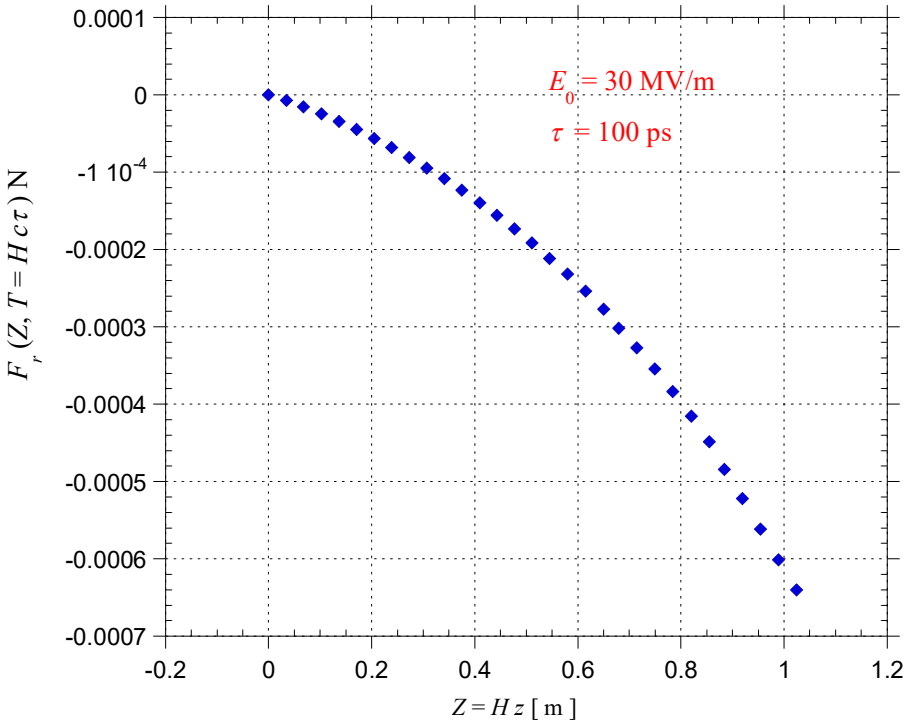

FIG. 7. Transverse component of the force acting on the beam as a function of the reduced coordinates Z along the axis of the RF-gun at the end of photoemission (at time T = Hcτ).

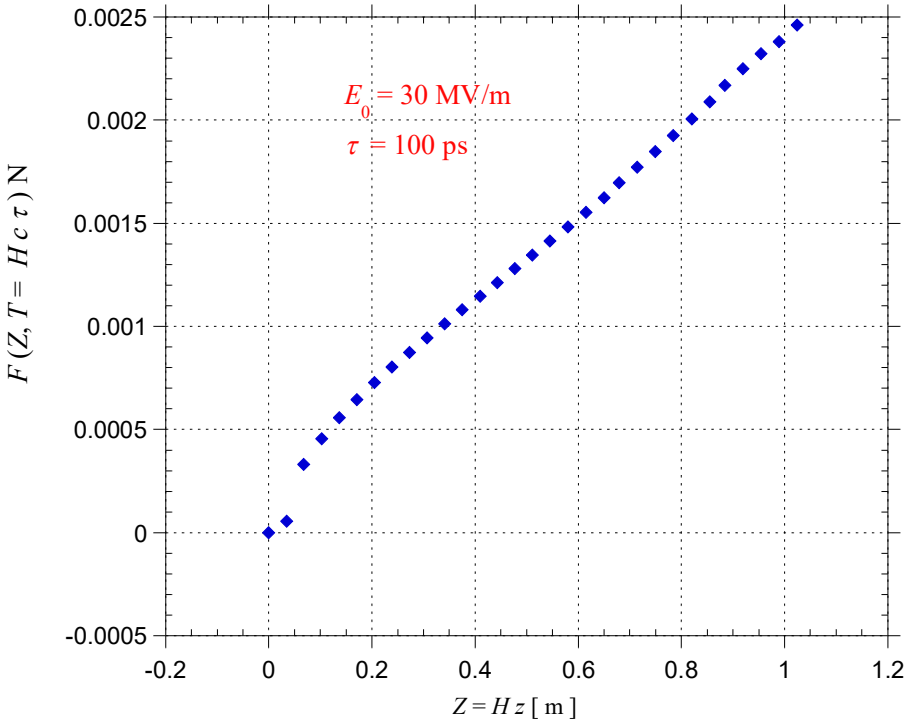

FIG. 8. The magnitude of the total force acting on the beam as a function of the reduced coordinates Z along the axis of the RF-gun at the end of photoemission (at time T = Hcτ).

All of these figures and Equation (19) reveal two effects on the beam: the first one, due to the longitudinal component of the force, affecting the trailing electrons in the beam, changes the energy of individual electrons in the beam, depending on their position. Consequently, the short-range wakefield induces energy spread in the beam.

The second effect, due to the transverse component of the force, deflects the beam trajectory. The electrons within the beam are decelerated by the positive charge image field. Consequently, these electrons lose more energy than those situated at the beam head. The negative transverse force illustrated in Figs. 4 and 7 means that this force is defocusing. The electrons within the beam experience over the beam length an average deflecting force that is proportional to the radial displacement r ($0 < r < a$) and dependent on the distance z. Figs. 3 to 8 show that the short-range space charge forces move together with the beam. They are not constant along the RF-cavity. Therefore, in a single bunch beam, the transverse wake forces from the bunch head deflect the tail of the beam; this deflection works towards distorting the beam into a *banana*-like shape in the initial stage of the acceleration and a spherical one at the exit aperture of the RF- cavity.

Conclusion

We have shown that it is possible to investigate numerically the force acting on an accelerated electron beam in the initial stage of acceleration, during the photoemission of the electrons from the cathode. The formula of the Lorentz force is expressed as an integral form of the components of the wakefield over the entire beam volume.

The components of wakefield generated by an accelerated electron beam that has just been emitted from the cathode in a “Pill-Box” cavity are derived from the Lienard-Wiechert potential and the method of images during the photoemission of the electron beam from the cathode [24].

Numerical calculations of the beam wakefield forces revealed two major effects on the beam: the first one is ascribed to the longitudinal component of the force, which affects the trailing electrons in the beam and changes the energy of the individual electrons, depending on their position. As a result, the short-range longitudinal component of the wakefield force will give rise to energy spread in the beam.

The second effect, due to the transverse component of the force, deflects the beam trajectory. The electrons within the beam experience over the beam length an average deflecting force that is proportional to the radial displacement r ($0 < r < a$) and dependent on the distance z. This deflection might lead to the tilting of the tail of the beam into a nearly "*banana*" shape in the initial stage of the acceleration and a spherical one at the exit of the RF-gun. Particle loss will occur when the tilted beam hits the cavity's lateral wall. This would be the cause of the beam breakup.

Since the forces that onset the electrons beam emanate from the beam itself, our numerical results and discussion of these forces represent a significant step towards an advanced understanding of wakefield accelerator technology [27-29]. These results could be an important background reference for the experimental layout and design of laser-driven plasma wakefield accelerators [30].

References

[1] Madey, J.M., J. Appl. Phys., 42(5) (1971) 1906.

[2] Deacon, D. et al., Phys. Rev. Lett., 38 (1977) 892.

[3] Carlsten, B.E. et al., J. Phys. B: At. Mol. Opt. Phys., 47 (2014) 234012.

[4] Hartemann, F.V. et al., Rev. Spec. Top. Accel. Beams, 8 (2005) 100702.

[5] Hartemann, F.V. et al., Laser Part. Beams, 22 (2004) 221.

[6] Di Mitri, S. and Cornacchia, M., Phys. Rep., 539 (2014) 1.

[7] Di Mitri, S., Photonics, 2 (2015) 317.

[8] Schaer, M. et al., Phys. Rev. Accel. Beams, 9 (2016) 072001.

[9] Kikuchi, T. et al., Phys. Rev. Accel. Beams, 19 (2016) 06420.

[10] Davidson, R.C. and Qin, H., "Physics of Intense Charged Particle Beams in High-Energy Accelerators", (Imperial College Press, Singapore, 2001).

[11] Wangler, T.P., "RF Linear Accelerators", (Wiley-VCH, New York, 2008).

[12] Reiser, M., "Theory and Design of Charged Particle Beams", (Wiley, New York, 1994).

[13] Reiser, M., J. Appl. Phys., 70 (1991) 1919.

[14] Kapchinskij, J.M. and Ladimirskij, V.V., Proc. International Conference on High Energy Accelerators, (CERN 274, 1959).

[15] Fraser, J.S. et al., Particle Accelerator Conference PAC85, 1791 (1985).

[16] CST GmbH, Bad Nauheimer Strasse 19, D-64289, Darmstadt, Germany.

[17] Floettmann, K., ASTRA User Manual, www.desy.de/~mpyflo/Astra_dokumentation. Accessed on Sep. 09, 2017.

[18] Nogales, J. et al., Radio Sci., 47 (2012) RS5006.

[19] Salah, W. and Dolique, J-M., Nucl. Inst. and Meth. A, 431 (1999) 27.

[20] Salah, W. et al., Nucl. Inst. and Meth. A, 564(1) (2006) 66.

[21] Salah, W. and Dolique, J-M., Nucl. Inst. and Meth. A, 447 (2000) 309.

[22] Salah, W. and Hallak, A.B., J. Phys. D, Applied Physics, 38 (2005) 2292.

[23] Salah, W., Nucl. Inst. and Meth. A, 480 (2002) 398.

[24] Salah, W. et al., Nucl. Inst. and Meth. A, 607 (2009) 498.

[25] Kim, K.-J. et al., J. Appl. Phys., 68 (1990) 4942.

[26] Figuera, H. et al., Phys. Rev. Lett., 60 (1988) 2144.

[27] Adli, E. et al., New J. Phys., 18 (2016) 103013.

[28] Floettmann, K., Phys. Rev. Spec. Top. Accel. Beams, 18 (2015) 064801.

[29] Guillaume, E. et al., Phys. Rev. Lett., 115 (2015) 155002.

[30] Litos, M. et al., Nature, 515 (2014) 92.